

Analysis of the cytochrome distribution *via* linear and nonlinear Raman spectroscopy

Angela Walter,^a Susann Erdmann,^b Thomas Bocklitz,^a Elke-Martina Jung,^b Nadine Vogler,^c Denis Akimov,^c Benjamin Dietzek,^{ac} Petra Rösch,^a Erika Kothe^b and Jürgen Popp^{*ac}

Received 8th October 2009, Accepted 19th February 2010

First published as an Advance Article on the web 12th March 2010

DOI: 10.1039/b921101b

The cytochrome distribution in hyphal tip cells of *Schizophyllum commune* was visualized using resonance Raman mapping and CARS microscopy. For comparison, resonance Raman mapping and CARS imaging of cytochrome was also performed during branch formation and in completely developed central hyphae. Cytochrome, as an essential component of the electron transport chain in mitochondria, plays an important role in providing energy to actively growing mycelia. It could be shown that mitochondria at the growing hyphal tips and at branching regions are more active, *i.e.* contain more cytochrome, as compared to those in older parts of the hyphae. This finding is compatible with the idea of high energy consumption for biosynthesis and intracellular transport at the growing tip, while older hyphae have lower needs for ATP generated *via* the respiratory chain in mitochondria. To the best of our knowledge this is the first study reporting about the localization and distribution of cytochrome, as an indirect mitochondria localization within *S. commune* or other basidiomycetous fungi, by means of resonance Raman microspectroscopy and CARS microscopy. These Raman methods bear the potential of label-free *in vivo* mitochondria localization and investigation.

Introduction

Filamentous fungi grow exclusively by apical extension of hyphae. The hyphal apex contains large numbers of small transport vesicles which accumulate and form the vesicle supply center, which plays an important role in hyphal growth by supplying the growing hyphal tip with enzymes and chemical building blocks.¹ The involvement of vesicles supplying cell wall material and membrane lipids to the growing tip has been extensively characterized in ascomycetes, where the “*Spitzenkörper*” can be easily seen in light micrographs. In basidiomycetes, the vesicle supply center is not that easily visible. For the model basidiomycete *Schizophyllum commune* (*S. commune*), the role of a vesicle supply center in hyphal growth has been demonstrated and a model for apical growth has been established^{2–4} (Fig. 1A). *S. commune* is well investigated for mating interactions^{5,6} and cell differentiation^{7–10} by microbiological and molecular methods and can easily be grown on artificial media.^{5,11} Fully grown hyphae in the central mycelium appear often highly vacuolated and the nucleus is located approximately at the median. Branching in such older hyphae re-establishes a new region of localized, apical hyphal growth. Within fungal mycelia, an inhomogeneous distribution of cell components is observed. The chemical composition of filamentous cells varies due to the different ages and functions between

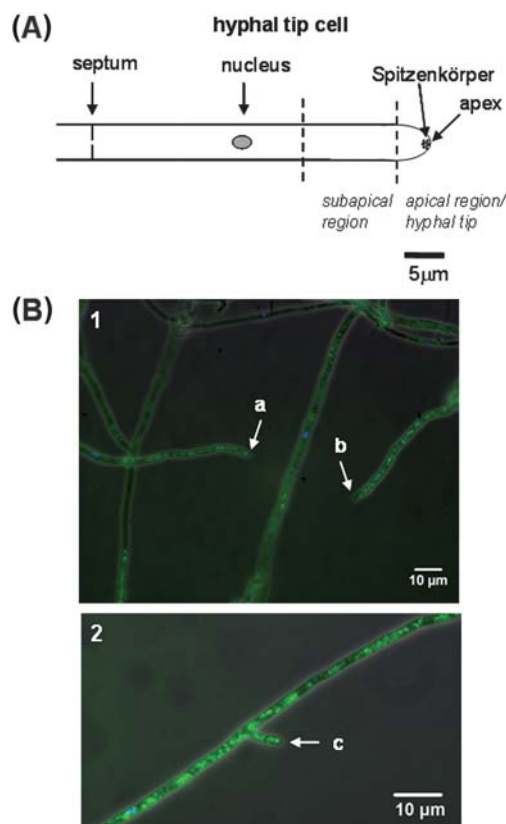


Fig. 1 Schematic drawing of a hyphal tip cell (A) from the apex containing the “*Spitzenkörper*” and the subapical region to the first septum. The nucleus is approximately located at the center of the cell. Mitochondria staining (B) by the fluorescent dye Mitotracker Green including hyphal tip cells a, b (1) and a branch c (2) of *Schizophyllum commune*.

^aInstitute of Physical Chemistry, Friedrich Schiller University, Helmholtzweg 4, 07743 Jena, Germany. E-mail: juergen.popp@uni-jena.de; Fax: (+49)3641 948302; Tel: (+49)3641 948320

^bInstitute of Microbiology, Friedrich Schiller University, Neugasse 25, 07743 Jena, Germany

^cInstitute of Photonic Technology, Albert Einstein Str. 9, 07745 Jena, Germany

and within hyphal sections. Mitochondria are visible throughout cells of all ages. In this regard, it is possible that mitochondria are either more active at the growing tip or that there are more mitochondria present. In electron micrographs of *S. commune* performed with respect to other questions, no accumulation of mitochondria at the tip was visible.¹² The visualization of mitochondria is commonly achieved within microbiology by fluorescence microscopy applying fluorescence labels and thus requiring extensive sample preparation. Here we will show that the vibrational spectroscopic Raman techniques resonance Raman mapping and Coherent anti-Stokes Raman scattering (CARS) microscopy are an alternative to fluorescence microscopy to visualize intracellular substance distribution offering the advantages of being label-free, minimal invasive and easy to implement. Raman based methods have emerged in the last few years as an extremely powerful method in biology or biomedicine.^{13–21} The principle is that Raman spectra contain information on molecular vibrations that provide a highly specific fingerprint of the molecular structure and biochemical composition of cells, tissues *etc.* That way Raman microspectroscopy has been successfully applied to study biological samples in their natural environment^{22,23} *e.g.* alkaloids in plant cells.^{24–28} The investigation of microorganisms such as bacteria^{29–37} and yeasts^{38–42} by means of Raman microscopy has been established and improved to the level of a single cell analysis.^{43–52} Furthermore vibrational spectroscopy has been used to study the chemical compounds involved in cell differentiation of *S. commune*^{53,54} or which are produced by *S. commune* itself.⁵⁵ In addition, vibrational spectroscopic characterization of fruiting bodies⁵⁶ and Raman spectroscopical studies of fungi⁵⁷ and spores^{58,59} have been carried out. The combination of Raman spectroscopy with chemometrical methods is capable to identify spores of macrofungi/basidiomycetes.⁶⁰ Recently, *S. commune* has been detected in wood and discriminated from another wood decaying fungal species by FTIR spectroscopy⁶¹ and a classification at strain level was achieved.⁶² Raman spectroscopy in combination with a light microscope can be applied as an imaging/mapping technique providing spatially resolved chemical information with a resolution below 1 μm . Thus Raman mapping is a suitable tool to generate chemical images of molecules in two or three spatial dimensions *e.g.* of secondary metabolites in plants.⁶³ Raman and surface enhanced Raman scattering (SERS) maps of *Aspergillus nidulans* hyphae grown on nanostructured gold-coated substrates have been recorded.⁶⁴ All these examples demonstrate that Raman microspectroscopy is capable of visualizing the chemical composition within a cell without the need of external labels which may adversely affect the living biological system. However, while the specificity of Raman spectroscopy is very high its sensitivity *i.e.* the conversion efficiency of the Raman effect is rather poor. Therefore, Raman microspectroscopy cannot be applied to record Raman maps in real time *i.e.* with video rate and is only applicable to study problems where time plays no role.

To overcome this disadvantage of low sensitivity, special Raman signal enhancing techniques exist. The two most prominent approaches are the resonance Raman effect⁶⁵ and the surface enhanced Raman scattering (SERS).⁶⁶ Besides these two linear Raman signal enhancing techniques a nonlinear variant of Raman spectroscopy called coherent anti Stokes Raman

spectroscopy (CARS) belongs to the most promising Raman techniques because it combines signal enhancement due to the coherent nature of the process with further advantages such as directional emission, narrow spectral bandwidth and no disturbing interference with autofluorescence.^{67,68} In order to generate a CARS signal two laser beams at a pump and a Stokes frequency are tightly focused onto the sample producing a signal at the anti-Stokes frequency. As the CARS signal is generated in a nonlinear process, the signal originates from the small spatial volume where the fields are highest. This leads to a method with intrinsic high spatial resolution and 3D sectioning capability. In addition, CARS imaging in contrast to the conventional linear Raman techniques achieves measurement periods in time scales of video rates. CARS imaging is widely applied in material sciences,⁶⁹ analytics^{70,71} and life sciences.^{72–75}

Here, Raman microspectroscopy and in particular resonance Raman mapping and CARS microscopy were used to map cytochromes in the mitochondrial membrane. For comparison, mitochondria were stained in living cells of *S. commune* with a mitochondrion-selective fluorescent dye and the distribution of mitochondria was compared to intensities of cytochrome Raman mapping. *S. commune* was chosen due to its significance within the microbiological field, especially for mycological studies concerning the complex reproductive cycle.^{6,76,77} Additionally, *S. commune* gains importance for bioremediation application.^{78,79}

Experimental

Strains and growth

S. commune 12–43 (*matA*_{3,5}; *matB*_{2,2}; *ural*⁻; Fungal Reference Center, University of Jena, Germany) was cultured at 28 °C for 3–6 days on solid medium (CYM: 2 g trypticase peptone, 2 g yeast extract, 20 g glucose monohydrate, 0.5 g MgSO₄·7H₂O, 0.5 g KH₂PO₄, 1.31 g K₂HPO₄·3H₂O and 18 g agar-agar per litre of distilled water) with a glass cover slip (fluorescence microscopy) or a fused silica slide (Raman microscopy) onto the agar. After 2–3 days at 28 °C, mycelium of *S. commune* was grown over the slide with a monolayered growth front. For the Raman spectroscopy, the slide was removed directly before the measurements and kept under room conditions during the spectroscopic analysis.

Fluorescence microscopy

Localization of mitochondria in living *S. commune* hyphae was performed using Mitotracker Green (Molecular Probes, Invitrogen, The Netherlands). The hyphae were incubated with 25–40 nM Mitotracker Green in liquid CYM for 40 min at 28 °C. Microscopy was carried out with an Axioplan 2 microscope (filter set 10: ex BP 450–490/em BP 515–565, Zeiss, Jena, Germany). Nuclei were stained with DAPI (1 μM 4',6-diamidino-2-phenylindole-dihydrochloride in embedding medium: 0.1 M Tris-HCl pH 8.0, 50% glycerol and 1 mg/mL phenylene diamine) and detected with filter set 2 (ex G 365/em LP 420). Documentation was achieved with a digital camera (Insight Firewire 4 image sample, Diagnostic Instruments, Sterling Heights) and analyzed by the software Spot (version 4.6, Diagnostic Instruments, Sterling Heights).

Raman spectroscopy

Raman measurements were carried out with a micro-Raman setup (HR Labram invers; Jobin Yvon, Horiba) combining a spectrometer with a focal length of 800 mm and a 300 lines per mm grating with an inverse Olympus microscope BX41. The entrance slit of the spectrometer was set to 100 μm and the Raman scattered light was detected by a Peletier cooled, back-illuminated CCD camera (1024 \times 512 pixel). The spectral resolution was approximately 6 cm^{-1} . With this spectral resolution a complete Raman spectrum is processed at once which is for the benefit of measurement time. The Raman spectra were obtained with an excitation wavelength of 532 nm from a frequency doubled Nd:YAG-Laser (Coherent, Dieburg, Germany). The laser beam was focused by a 100 \times microscope objective (PL Fluotar L100 \times 0.75; Leica) with a working distance of 4.7 mm and a numerical aperture of 0.75 onto the sample with a net power of about 3 to 5 mW on the sample and an approximated diameter of 1 μm . For the Raman mapping experiments the samples were moved by an x/y motorized stage (Märzhäuser, Wetzlar, Germany) with a minimal step size of 0.1 μm . The step-size of the Raman map was configured to 0.7 μm in x and y directions and the integration times were chosen to be 45 s for each measured spectrum during the Raman mapping.

The Raman spectrum of human cytochrome b5 has been used as reference for cytochromes bound to the mitochondrial membrane. Spectra were processed with LabSpec software (Horiba Jobin-Yvon, Benzheim, Germany). For intensity plots of the Raman maps, the spectra were baseline corrected, approximated by linear segments with manually chosen points and the images were smoothed by the LabSpec software.

The CARS microscopy setup used was described previously by Meyer *et al.*⁶⁹ Differently from previous work we used only a single optical parametric oscillator (OPO; APE, Germany) for generation of the pump pulse, while the output of the Ti:sapphire oscillator (Coherent Mira HP) was used as the source for the Stokes pulses. The beams was focused using a NA 0.95 50 \times objective (Zeiss) and the CARS signal was collected by a NA 0.55 condenser. Filters separated the CARS signal from the residual pump and Stokes light and detection has been carried out by a photomultiplier (Hamamatsu R6357). The data acquisition time for the CARS images reported herein (size: 512 \times 512 pixels) did not exceed 25 s. CARS image series have been recorded by varying the spectral shift between the pump and the Stokes pulses thereby spectrally covering the spectral region between 1552 and 1626 cm^{-1} characteristic for cytochrome and at 2990 cm^{-1} to monitor the spatial distribution of aromatic and aliphatic C–H stretching modes.

Data analysis

In order to evaluate the spatial distribution of chemical substances in Raman maps, chemometrical analysis was applied. A k -means clustering analysis⁸⁰ implemented in the statistical language R⁸¹ was used. For data preprocessing cosmic ray removal, baseline correction, vector normalization and truncation to the wavenumber region from 2149 cm^{-1} to 299 cm^{-1} were performed. The number of clusters, k , was set to six. The algorithm started with a random distribution and the spectral

distances to the mean of all clusters were calculated and the indexing was renewed according to the minimal distance. This was repeated until a stable arrangement was reached. The clusters are color coded and the spatial distribution of the clusters was plotted. For visualization of the cytochrome distribution, relative band maxima intensity ratios between the peaks at 1652 and 1573 cm^{-1} were calculated. In doing so the peak intensity of the band located around 1573 cm^{-1} was normalized by the value of the band maximum of 1652 cm^{-1} (for an assignment of these Raman peaks see section, Results and discussion).

Results and discussion

Mitochondria distribution in hyphae

A simplified schematic sketch representing a hyphal tip cell of *S. commune* is shown in Fig. 1A. The apical region of a hyphal tip cell extends from 2 to 5 μm from the apex and is featured by the “Spitzenkörper”, an accumulation of vesicles, responsible for supplying the growing hyphal tip with enzymes and chemical building blocks. Mitochondria can be mainly found in the subapical regions, about 10 to 15 μm behind the apex. Central regions of tip hyphae show more vacuoles and the nucleus is approximately located in the middle of the cell, while the length of the hyphal tip cell is bounded by the first septum. In branching regions, typical for subapical regions, vesicles and mitochondria are accumulated. Within the fungal cells an inhomogeneous distribution of cell components was observed. The chemical composition of filamentous cells varies due to the different functions of the hyphal section.

The microscopic inspection revealed a unilayered, nicely distinguishable growth front which could be used to visualize intracellular components. Mitochondria were visualized and set apart from other organelles using the mitochondrion-specific fluorescent dye Mitotracker Green (Fig. 1B). The mitochondria are observed in all regions of hyphae including growing hyphal tips (1a, b) and branching region (2c). Mitochondria occur equally distributed along all hyphal parts within the mycelium. In a few cases, accumulations of mitochondria were observed. Specifically, no accumulation of mitochondria was observed in growing tips or branches by fluorescence microscopy. The occurrence of distribution pattern of mitochondria stained by Mitotracker observed in this study correlates with the results of studies in other filamentous fungi.^{82–85}

Distribution of cytochromes

Raman mapping was performed on a hyphal tip of *S. commune* by recording the Raman spectra within the marked area displayed in the microscopic image in the inset of Fig. 2. The length of the mapped hypha was approximately 23 μm to cover the region from the apex to the subapical region. Spectrum a_1 in Fig. 2A displays a typical Raman spectrum recorded within the apical region of the hyphal tip cell while spectrum a_2 represents a Raman spectrum taken in the subapical region further away from the hyphal tip. The most prominent band in the two Raman spectra shown in the upper panel of Fig. 2A centered at 2924 cm^{-1} can be assigned to an asymmetric CH-stretching vibration of methylene groups from all cell constituents.⁸⁶ The

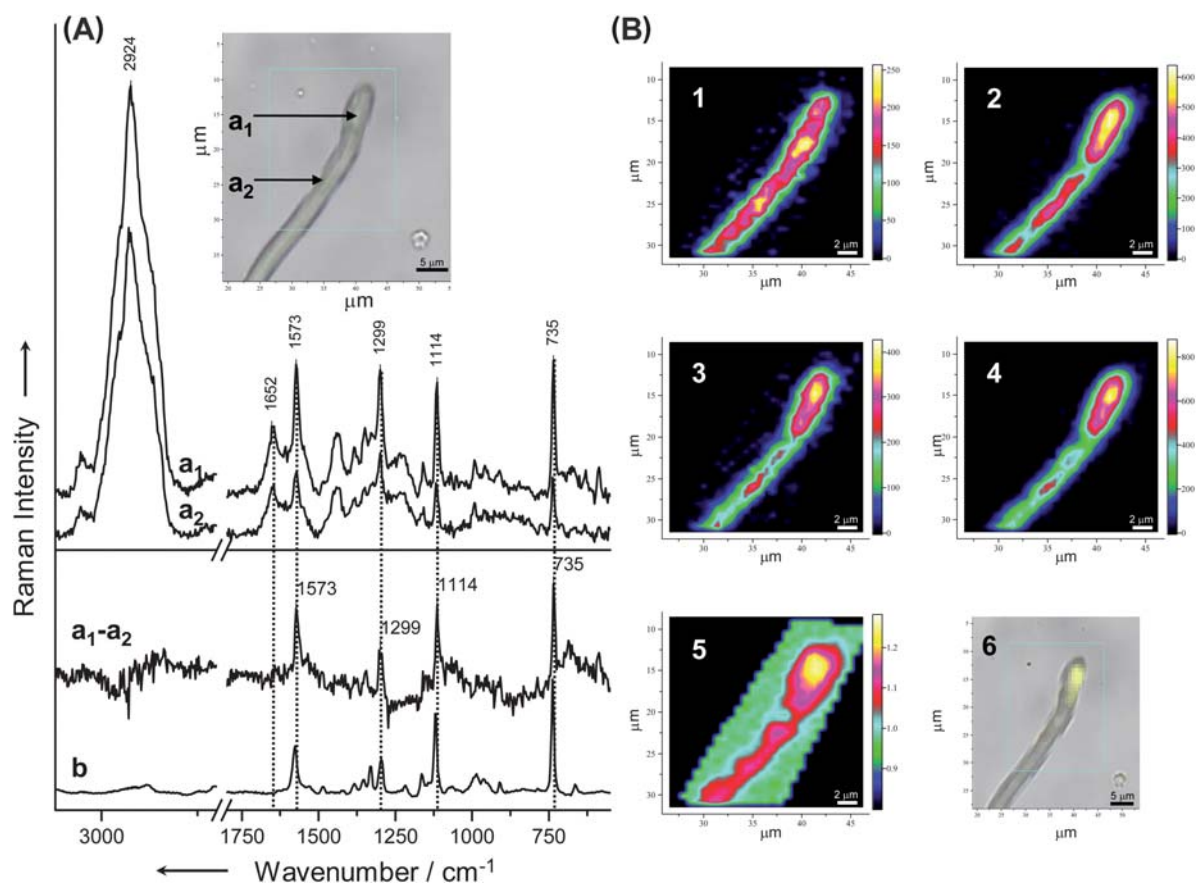


Fig. 2 (A) Representative Raman spectra of a hyphal tip cell of *S. commune* (microscopic picture is depicted in the inset) at the two different locations a_1 and a_2 , the difference spectrum ($a_1 - a_2$) and the cytochrome b reference spectrum. (B) Intensity distribution of the Raman band representing matrix content by the central peak position at 1652 (1) and cytochrome marker bands with the central peak position at 1573 (2), 1114 (3), 735 cm^{-1} (4). The relative cytochrome to matrix content is depicted by the relative intensity ratio of the bands centered at 1573 and 1652 cm^{-1} (5) and the overlay of the microscopic picture and the relative intensity ratio of 1573 to 1652 cm^{-1} (6). The plotted intensity distributions are smoothed by the LabSpec software. Bar: 2 μm for B1–5 and 5 μm for B6.

Raman band located at 1652 cm^{-1} results from a superposition of protein, lipid and polysaccharide vibrations and is therefore a marker of all relevant cell substances *i.e.* is typical for the fungal cell matrix and is used throughout this work as a reference band for normalization.^{57,60,87} Raman bands due to DNA and RNA vibrations are negligible for the applied Raman excitation wavelength of 532 nm. The Raman bands at 1573, 1299, 1114 and 735 cm^{-1} can be assigned to cytochrome vibrations as can be seen by comparison with the cytochrome reference spectrum, labeled b in the lower panel of Fig. 2A. Cytochromes are hemoproteins consisting of an iron ion coordinated to a porphyrin cycle which is composed of a conjugated π system of 4 pyrrole rings interconnected by vinyl groups. The electronic absorption spectrum of cytochromes exhibits an intense Soret band around 400 nm and additional α and β bands between 500 and 560 nm.⁸⁸ The Raman excitation wavelength of 532 nm was chosen to be resonant with the electronic absorption of cytochrome in order to achieve a selective resonance Raman enhancement of the Raman modes of the cytochrome chromophore. The porphyrin in-plane C=C stretching motion of the porphyrin skeleton of cytochromes is commonly located around 1570 cm^{-1} and occurs in the Raman spectra a_1 and a_2 of Fig. 2A

at 1573 cm^{-1} . The deformation modes of CCC and CNC bonds of the chromophore are positioned at 1114 cm^{-1} and 735 cm^{-1} . The Raman signal at 1299 cm^{-1} is due to cytochrome ring modes that are coupled with the peripheral vinyl groups. These Raman bands have been reported as signals of b-^{89–91} or c-type cytochromes^{91,92} and of b*c-complex cytochromes.⁹³

The Raman spectra a_1 and a_2 in Fig. 2A exhibit similar signal patterns but differ in band intensities. To visualize the differences between the two fungal Raman spectra (a_1 and a_2) a difference spectrum was calculated by subtracting the normalized and baseline corrected spectrum a_1 from spectrum a_2 . The difference spectrum labeled as $a_1 - a_2$ in Fig. 2A exhibits the bands positioned at 1573, 1299, 1114 and 735 cm^{-1} thus showing the same characteristic Raman signals as the cytochrome reference spectrum b in Fig. 2A.

It has been reported that *S. commune* contains b-type and c-type cytochromes.⁷⁶ The Raman spectra of mitochondria published by Adar and Erecinska⁹³ are very similar to the Raman spectrum a_1 of *S. commune* and the difference spectrum ($a_1 - a_2$) shown in Fig. 2A. Therefore, we assume that the cytochrome distribution corresponds to the localization of active mitochondria within the mapped area of the *S. commune* hypha.

Raman spectroscopical investigations of mitochondria have been carried out before, but not under resonant conditions for cytochrome and mitochondria activity.^{94,95}

To generate spatially resolved Raman information within the hyphal tip cell, Raman mapping was applied. Within the mapped area shown in the microscopic picture in Fig. 2A, a complete Raman spectrum was recorded for each measured point. The false color plots visualize the intensity distribution of typical marker bands (Fig. 2B) derived from baseline corrected Raman spectra. Image 1 displays the intensity distribution of the Raman band at 1652 cm^{-1} *i.e.* displays the cell matrix. Black regions are due to negligible Raman intensities of the substrate material while the areas containing substantial fungal information are displayed by the colors: blue, green, red to yellow where the intensities increase from blue to yellow. The intensity plot of the Raman signal located at 1652 cm^{-1} (Fig. 2B1) exhibits the highest intensities in the hyphal center (red to yellow) and low intensities at the rim of the hypha (blue to green) while the intensity distribution appears nearly homogeneous along the hypha. The variations along the hypha present in the false color plot of the matrix content (1652 cm^{-1}) are mainly due to the heterogeneity of the eukaryotic cell as well as varying sample thickness and the resulting variation of the confocal plane. The tubular shape of the hypha and the slight height inhomogeneities of the hypha are

responsible for the different amounts of sample material within the laser focus between the hyphal center and the rim. The cytochrome distribution is represented by the intensity plots of the cytochrome marker bands located at 1573 , 1114 and 735 cm^{-1} (images 2, 3 and 4 in Fig. 2B). These intensity plots of the cytochrome marker bands show an apical increase, which is highlighted by normalizing the intensity plot of the 1573 cm^{-1} mode by the cell matrix plot *i.e.* the 1652 cm^{-1} distribution. Such a normalized cytochrome distribution image is depicted in the image 5 of Fig. 2B. The intensity variations of the matrix marker band are smaller as compared to the concentration differences of cytochrome. In image 6 of Fig. 2B the microscopic picture of the fungal hypha is superimposed by the intensity distribution of the relative band ratio plot shown in image 5. The yellow regions illustrate the areas of highest relative intensity of the 1573 cm^{-1} signal within the apical region of the hyphal tip cell.

Visualization of cytochrome contents in different compartments of the hyphae

The investigation of the cytochrome distribution has been extended from the hyphal tip to branches, creating new centers of mycelial growth and fully grown compartments in the middle of a grown hypha. In Fig. 3 the microscopic picture of a branching

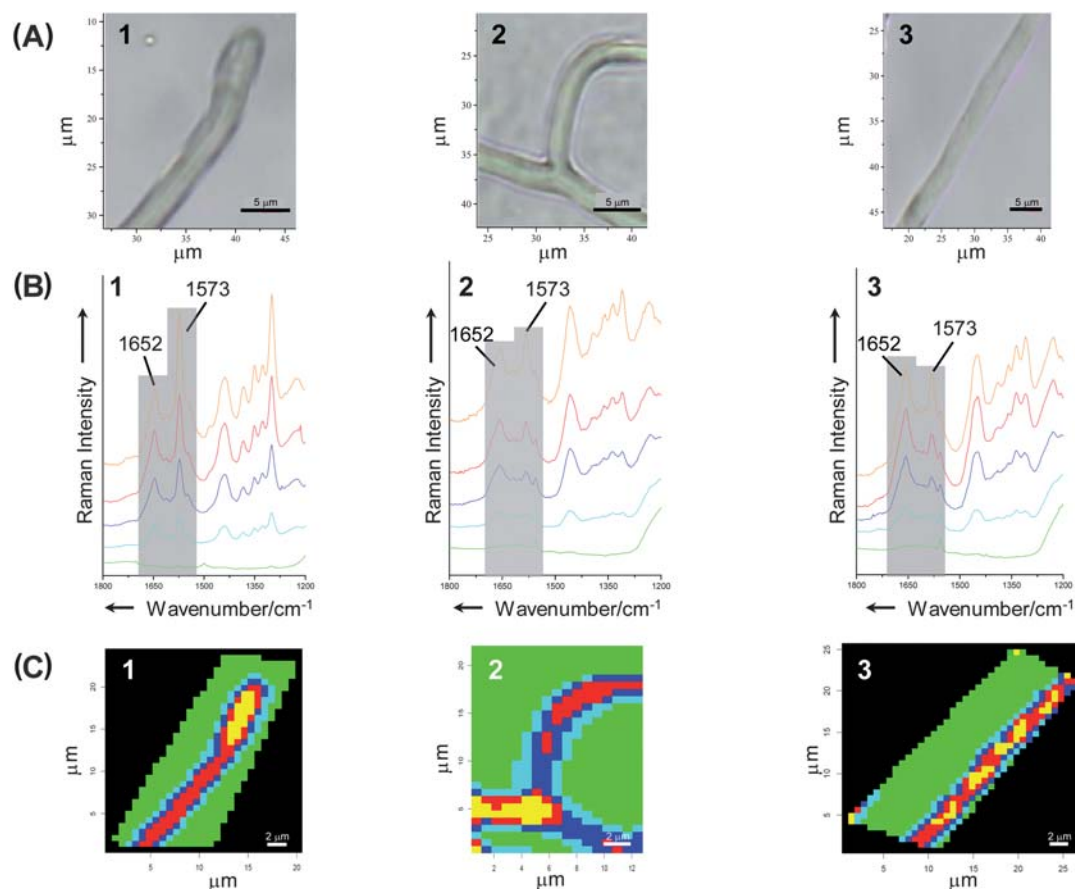


Fig. 3 Panel A shows the microscopic pictures of the hyphal tip cell (image 1), the branching region (image 2) and the fully grown central hypha (image 3). Panel B contains the mean Raman spectra of the *k*-mean cluster analysis including the spectrum of the hyphal tip cell (spectrum 1), of the branching region (spectrum 2) and the central hyphal compartment (spectrum 3). The spectra contain the most relevant spectral region concerning the cytochrome (1573 cm^{-1}) to protein (1652 cm^{-1}) content. The distributions of the clusters are plotted as false color images in panel C (1–3) and the color coding correlates to the spectra B1–3. Bar: $5\text{ }\mu\text{m}$ for A1–3 and $2\text{ }\mu\text{m}$ for C1–3.

region (A2), a central compartment (A3) next to the hyphal tip cell (A1) are presented. In order to achieve a better interpretation and visualization *k*-mean cluster analysis has been applied to analyze the Raman images. The relevant sections of the mean spectra are depicted in row B of Fig. 3 demonstrating the grouping characteristics most clearly. Spectrum 1 in panel B shows the mean cluster Raman spectra from the hyphal tip cell while in spectrum 2 and spectrum 3 the mean cluster spectra from regions of the branching area and the central compartment are displayed. The Raman signals at 1652 cm^{-1} and 1573 cm^{-1} due to the reference matrix signal and the cytochrome marker band are again used to monitor the cytochrome content within the mapped area. The mean spectra are colored in green, light blue, dark blue, red and orange with increasing intensity ratios of the 1573 to 1652 cm^{-1} Raman signals and therefore increasing cytochrome content. The intensity behavior of the other cytochrome signals located at 1299 , 1114 and 735 cm^{-1} correlate with the intensity of the cytochrome marker band at 1575 cm^{-1} (compare with Fig. 2A). The color coding of the mean spectra are consistent with the color coding of the false color images displayed in row C of Fig. 3. The areas where no Raman spectra

were recorded are displayed as black regions. The green areas display the substrate material within the Raman maps. The areas containing fungal spectra are color coded from blue to orange. The light blue spectra exhibit only weak spectral information and can be found at the cell periphery. The images reveal that the highest cytochrome content can be found within the apical region of the hyphal tip cell (C1) and before the branching point (C2) while the fully grown hypha shows a regular distribution within the central compartment (C3).

Estimation of relative cytochrome contents in different compartments of the hyphae

Fig. 4 illustrates the quantification of the relative cytochrome content at different hyphal compartments. The microscopic pictures of the analyzed parts are depicted in Fig. 4 panel A. The cytochrome content is depicted in Fig. 4 panel B and quantified in panel C. Fig. 4 panel B contains for visualization purpose the distribution of the absolute cytochrome content with individual intensity scales, exhibiting the cytochrome content within the hyphal compartments. To compare the cytochrome contents of

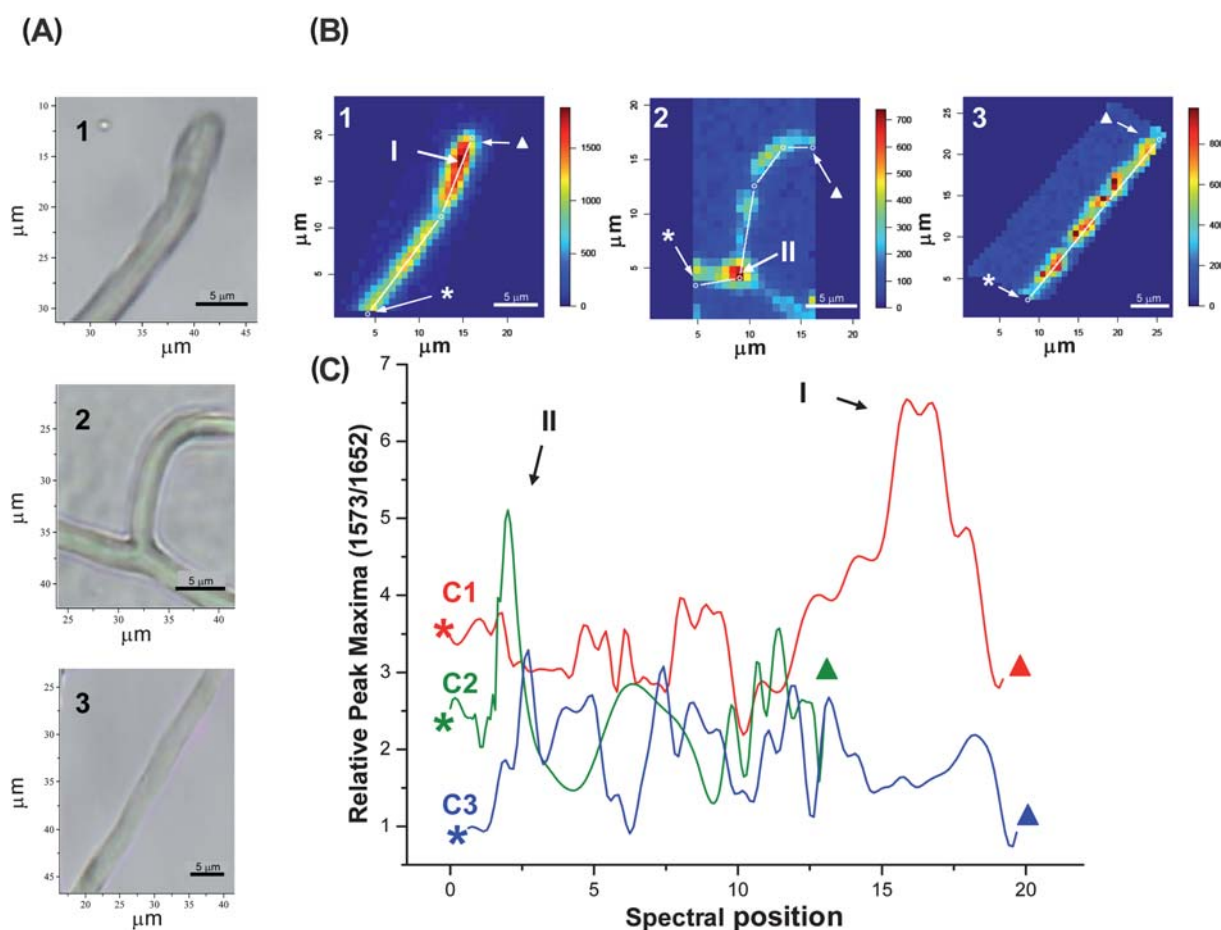


Fig. 4 (A) Microscopic pictures of a hyphal tip (A1), branching region (A2) and the fully grown hypha (A3). False color plots of the absolute intensity of the cytochrome marker band (1573 cm^{-1}) within the mapped regions of the hyphal tip cell (B1), the branching region (B2) and the central compartment (B3). The normalized cytochrome content is determined by the 1573 cm^{-1} to 1652 cm^{-1} ratio along the white line—beginning from star and ending at the triangle (see B1–3). The calculated intensity ratios are depicted as graphs C1, C2 and C3. The 2 cytochrome maxima I and II are highlighted in the graphs C1 and C2, respectively. Maximum I is located within the apical region of the hyphal tip cell (I in C1 and B1), whereas maximum II correlates with the branching spot of B2. For further details see section, Results and discussion. Bar: $5\text{ }\mu\text{m}$.

the different hyphal compartments the intensity values of the cytochrome marker band are normalized to a band which is related to the biomass. The results are depicted in one graph in Fig. 4C. Based on Fig. 2B picture 5 the assumption can be drawn that the absolute and relative cytochrome contents are closely related.

Fig. 4 visualizes an estimation of the different cytochrome contents over the mapped hyphal compartments for the hyphal tip cell (microscopic picture A1), for the branching region (microscopic picture A2) and for the central compartment (microscopic picture A3). The plots of absolute intensity distribution of the Raman mode 1573 cm^{-1} are depicted in Fig. 4 panel B as image B1 for the hyphal tip cell, image B2 for the branching region and image B3 for the central hypha compartment. The white lines mark the path which was used to determine the normalized cytochrome content. Starting point is marked by a star and the end is labeled by a triangle. The relative cytochrome (1573 cm^{-1}) to protein (1652 cm^{-1}) intensity ratio along this path is displayed in Fig. 4 as C1, C2 and C3. The ordinates of the graphs C1–C3 are rescaled for simplification to set the lowest values of the blue graph (C3) to about 1.

The relative cytochrome (1573 cm^{-1}) to protein (1652 cm^{-1}) intensity ratios exhibit maxima in the hyphal tip cell (Fig. 4C1) at the region I and at the branching region (Fig. 4C2) at region II, whereas the relative cytochrome to protein content is more regularly distributed over the central hyphal compartment (Fig. 4C3). The maxima of the graphs C1 (I) and C2 (II) correlate to the highlighted maxima I and II within the absolute intensity plots B1 and B2, respectively.

The intensity ratio ($1573\text{ cm}^{-1} : 1652\text{ cm}^{-1}$) monitoring the cytochrome content exhibits its highest value for the hyphal tip cell, featuring the maximum I which is located within the apical region. The branching area (maximum point II) exhibits slightly higher cytochrome content than the fully grown compartment where lower need of energy can be postulated. The cytochrome content within the middle compartment of a fully grown hypha (blue graph C3) is lower and appears to be distributed regularly, while the hyphal tip cell and the branching region show higher cytochrome contents. The branching spot (II) exhibits a threefold and twofold higher cytochrome content as compared to the average cytochrome content of the fully grown central hypha and the branch region, respectively. The relative cytochrome content of the hyphal tip cell (maximum I, red graph C1) is approximately seven times higher than the lowest cytochrome content of the central part of the hypha (C3). Thus, the cytochrome concentration is enhanced in growing regions of hyphae like hyphal tip (A1) and branching region (A2). Accordingly, we assume that the detection of cytochrome as a mitochondrial associated protein in the hyphal tip and in branching regions also reveals the localization of mitochondria in these regions. So, the occurrence of mitochondria in the hyphal tip as well as in branching regions correlates with the distribution of mitochondria in other filamentous fungi published elsewhere.^{84,85}

Visualization of cytochrome contents under real time conditions and increased spatial resolution

The localization of mitochondria distribution *via* cytochrome detection has been achieved by applying resonance Raman

spectroscopy exhibiting the advantages of minimal sample preparation, noninvasive measurement procedure, label-free technique and high specificity. Nevertheless, Raman mapping cannot be performed in real time, therefore dynamics in mitochondria distribution and mitochondria activity during hyphal growth cannot be observed. In contrast to linear Raman microspectroscopy, coherent anti-Stokes Raman scattering (CARS) allows for recording the distribution of a characteristic Raman mode within the sample with video rate. In the following we will show the potential of CARS microscopy to visualize the cytochrome distribution, thereby providing a benchmark step towards the online imaging of mitochondria distribution and mitochondrial activity.

CARS images of the fungal hyphae are shown in Fig. 5. Panel A of Fig. 5 depicts a CARS image recorded at 1572 cm^{-1} . As can be seen in Fig. 5A tuning the CARS signal to the cytochrome resonance at 1572 cm^{-1} yields a strong signal at the hyphal tip (I) and at the branching point (II), therefore reflecting the cytochrome distribution within the hypha. According to Fig. 5A the fully grown hypha (III) exhibits regular cytochrome content without any enhanced signal as can be seen for the hyphal tip (I) and the branching region (II). Panel B of Fig. 5 shows in image 1, the hyphal tip cell (I) and in image 2, the branching region (II) as well as parts of a central hypha (III) (seen in image 1 and 2) recorded at a Raman shift of 1552 cm^{-1} , establishing non-resonant conditions for the cytochrome marker Raman band at 1573 cm^{-1} . This cytochrome-related signal disappears under non-resonant conditions, *i.e.* the energetic difference between the pump and the Stokes-pulses are chosen not to coincide with a Raman-active vibration. The different brightnesses observed in Fig. 5 of the hyphal tip (I) and the branching region (II) under resonant (Panel A) and under non-resonant conditions (Panel B) clearly indicate the chemical information content in the contrast mechanism of CARS microscopy and stem from the molecular specificity of the CARS signal. The CARS image in Fig. 5A shows higher cytochrome content in the hyphal tip cell (I) and the branching region (II), reproducing the resonance Raman spectroscopic results discussed before (see Fig. 2B: image 5; Fig. 3: C1 and C2 and Fig. 4: B1/C1 and B2/C2). Whereas the central compartment (III) within Panel A of Fig. 5, shows no signal enhancement which indicates no specific increased cytochrome content, which supports the resonance Raman spectroscopic results (see Fig. 3C3 and Fig. 4B3/C3). Cytochrome accumulation has been detected within hyphal tips cells and branching regions *via* resonance Raman spectroscopy and CARS, whereas no accumulation of mitochondria could be determined within those regions by means of fluorescence microscopy. Since cytochrome is part of the respiratory system to generate ATP within the mitochondria, it can function as mitochondria activity marker. The detection of increased cytochrome content in specific regions and the detection of the mitochondria localization are not mutually exclusive. In growing hyphal regions more energy is demanded and so the mitochondria could be more active, *i.e.* contain more cytochrome.

In addition to CARS images recorded at 1572 cm^{-1} Fig. 5C displays CARS-microscopic images recorded in the CH-stretching region, which is widely used for the analysis of biological samples as it generally reflects the integrated content of organic materials. As is apparent from Fig. 5C at this

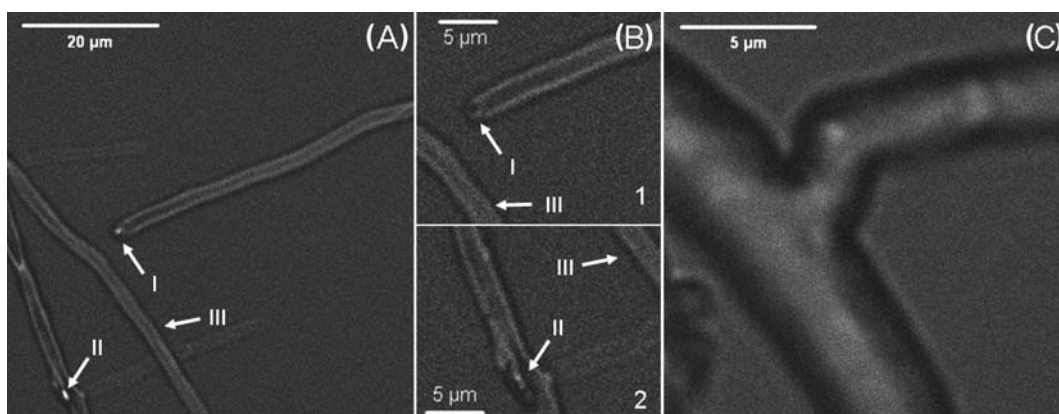


Fig. 5 CARS images of fungal hyphae. (A) CARS image of fungal hyphae recorded at 1572 cm^{-1} (cytochrome marker band, spectral resolution: 20 cm^{-1}). The arrows point to the hyphal tip (I), the hyphal branching (II) and the central hypha (III). In the tip and the branching higher cytochrome concentrations are observed indicated by the increased brightness. (B) The hyphal tip (I) (image 1), the branching (II) (image 2) and the central hyphal compartments (III) (images 1 and 2) recorded under non-resonant conditions (images were recorded at a Raman shift of 1552 cm^{-1}). The different brightnesses observed compared to the image in Panel A clearly indicate the chemical information content in the contrast mechanism of CARS microscopy. (C) CARS image of a hypha recorded at the CH stretching vibration (2990 cm^{-1}) showing the high resolution achievable (spectral resolution: 110 cm^{-1}).

Raman-shift no contribution of the cytochrome can be observed, however, it gives an indication of the spatial resolution that can be achieved with our setup. The field of view shows a hypha revealing a branching. The pixel size obtained is $30 \times 30\text{ nm}$. The spatial resolution of the CARS images is much higher compared to the spatial resolution of Raman microspectroscopy which is determined by the step size of $0.7\text{ }\mu\text{m}$ within the Raman maps. In principle both laserfoci are diffraction-limited in diameter.

The results of the CARS microscopic experiments support the findings of the resonance Raman study and show the great capability of using this nonlinear Raman based technique in conjunction with (resonance) Raman spectroscopy. However, CARS imaging allows for a significantly faster image acquisition rate than conventional Raman imaging, hence it shall develop into the method of choice for live imaging of biological processes. In this context the herein highlighted selectivity of the CARS process to cytochrome, by tuning the CARS process to be in resonance to a fingerprint vibration of the cofactor, provides a significant advance compared to imaging the global distribution of organic material or more specific proteins in general.³ The benchmark observation of cytochrome distribution by means of CARS microscopy reported here, will open the doorway for future studies, which aim at the online monitoring of cytochrome distribution and activity during the development of *S. commune*.

Conclusion

It has been shown that Raman and CARS microspectroscopy could be used as a label-free detection method for mitochondria in fungal hyphae. For cell investigations concerning metabolic activities mitochondria, as the energy supply center of the cell, are an important indicator for cell activity. The indirect visualization of mitochondria activity *via* cytochrome localization by means of resonance Raman and CARS microspectroscopy shows the potential of vibrational microspectroscopy for an *in vivo* tracking of intracellular processes. In contrast to conventional fluorescence microscopy and spectroscopy which is

e.g. able to localize mitochondria by Mitotracker staining, Raman and CARS microspectroscopy can be applied in a noninvasive manner *i.e.* are label-free and provide a molecular contrast. Resonance Raman spectroscopy provides beside the cytochrome information additional chemical characteristics due to the complex fingerprint region. While Raman imaging cannot be applied to monitor real time processes, CARS microscopy allows for recording images of one particular vibration with video rate. Thus CARS microscopy can be used in further research to retrieve additional specifications on mitochondrial function like *e.g.* on mitochondrial activity or to investigate *in vivo* the influence of environmental factors on mitochondria without the need of external labels. Mitochondria localization *via* cytochrome detection by means of resonance Raman imaging and CARS microscopy can possibly be transferred to other than fungal cells when the mitochondria have a specific component which is excited under resonant conditions.

Acknowledgements

We gratefully acknowledge financial support from the Deutsche Forschungsgemeinschaft (Graduiertenkolleg GK 1257 "Alteration and element mobility at the microbe-mineral interface" and Jena School of Microbial Communication – JSMC) and the Fonds der Chemischen Industrie.

References

- 1 G. Steinberg, *Eukaryotic Cell*, 2007, **6**, 351.
- 2 I. Rupes, W. Z. Mao, H. Astrom and M. Raudaskoski, *Protoplasma*, 1995, **185**, 212.
- 3 S. Bartnicki-Garcia, *Fungal Genet. Biol.*, 1999, **27**, 119.
- 4 S. N. Grove and C. E. Bracker, *J. Bacteriol.*, 1970, **104**, 989.
- 5 E. Kothe, *Appl. Microbiol. Biotechnol.*, 2001, **56**, 602.
- 6 E. Kothe, *Fungal Genet. Biol.*, 1999, **27**, 146.
- 7 M. L. de Vocht, K. Scholtmeijer, E. W. van der Vegte, O. M. H. de Vries, N. Sonveaux, H. A. B. Wosten, J.-M. Ruyschaert, G. Hadziioannou, J. G. H. Wessels and G. T. Robillard, *Biophys. J.*, 1998, **74**, 2059.

- 8 O. M. H. De Vries, W. H. C. F. Kooistra and J. G. H. Wessels, *J. Gen. Microbiol.*, 1986, **132**, 2817.
- 9 J. G. H. Wessels and D. J. Niederpruem, *J. Bacteriol.*, 1967, **94**, 1594.
- 10 H. A. B. Woesten, F. H. J. Schuren and J. G. H. Wessels, *EMBO J.*, 1994, **13**, 5848.
- 11 G. E. Palmer and J. S. Horton, *FEMS Microbiol. Lett.*, 2006, **262**, 1.
- 12 M. Raudaskoski, *Fungal Genet. Biol.*, 1998, **24**, 207.
- 13 M. Harz, M. Krause, T. Bartels, K. Cramer, P. Rösch and J. Popp, *Anal. Chem.*, 2008, **80**, 1080.
- 14 K. Maquelin, L. Dijkshoorn, T. J. K. van der Reijden and G. J. Puppels, *J. Microbiol. Methods*, 2006, **64**, 126.
- 15 M. S. Ibelings, K. Maquelin, H. P. Endtz, H. A. Bruining and G. J. Puppels, *Clin. Microbiol. Infect.*, 2005, **11**, 353.
- 16 M. Harz, R. A. Claus, C. L. Bockmeyer, M. Baum, P. Rösch, K. Kentouche, H. P. Deigner and J. Popp, *Biopolymers*, 2006, **82**, 317.
- 17 Q. Zhu, G. Quivey Robert and J. Berger Andrew, *J. Biomed. Opt.*, 2004, **9**, 1182.
- 18 A. J. Berger and Q. Zhu, *J. Mod. Opt.*, 2003, **50**, 2375.
- 19 Q. Zhu, R. G. Quivey, Jr and A. J. Berger, *Appl. Spectrosc.*, 2007, **61**, 1233.
- 20 K. Maquelin, L. P. Choo-Smith, H. P. Endtz, H. A. Bruining and G. J. Puppels, *J. Clin. Microbiol.*, 2002, **40**, 594.
- 21 K. Maquelin, C. Kirschner, L. P. Choo-Smith, N. A. Ngo-Thi, T. van Vreeswijk, M. Stammler, H. P. Endtz, H. A. Bruining, D. Naumann and G. J. Puppels, *J. Clin. Microbiol.*, 2003, **41**, 324.
- 22 R. Petry, M. Schmitt and J. Popp, *ChemPhysChem*, 2003, **4**, 14.
- 23 M. Schmitt and J. Popp, *J. Raman Spectrosc.*, 2006, **37**, 20.
- 24 E. Urlaub, J. Popp, V. E. Roman, W. Kiefer, M. Lankers and G. Rössling, *Chem. Phys. Lett.*, 1998, **298**, 177.
- 25 E. Urlaub, J. Popp, W. Kiefer, G. Bringmann, D. Koppler, H. Schneider, U. Zimmerman and B. Schrader, *Biospectroscopy*, 1998, **4**, 113.
- 26 T. Frosch, M. Schmitt, K. Schenzel, H. Faber Johan, G. Bringmann, W. Kiefer and J. Popp, *Biopolymers*, 2006, **82**, 295.
- 27 T. Frosch, M. Schmitt, T. Noll, G. Bringmann, K. Schenzel and J. Popp, *Anal. Chem.*, 2007, **79**, 986.
- 28 H. Schulz, M. Baranska, H.-H. Belz, P. Roesch, M. A. Strehle and J. Popp, *Vib. Spectrosc.*, 2004, **35**, 81.
- 29 K. Gaus, P. Rösch, R. Petry, K.-D. Peschke, O. Ronneberger, H. Burkhardt, K. Baumann and J. Popp, *Biopolymers*, 2006, **82**, 286.
- 30 U. Neugebauer, U. Schmid, K. Baumann, U. Holzgrabe, W. Ziebuhr, S. Kozitskaya, W. Kiefer, M. Schmitt and J. Popp, *Biopolymers*, 2006, **82**, 306–311.
- 31 U. Neugebauer, U. Schmid, K. Baumann, W. Ziebuhr, S. Kozitskaya, U. Holzgrabe, M. Schmitt and J. Popp, *J. Phys. Chem. A*, 2007, **111**, 2898.
- 32 E. C. Lopez-Diez and R. Goodacre, *Anal. Chem.*, 2004, **76**, 585.
- 33 L. P. Choo-Smith, K. Maquelin, T. Van Vreeswijk, H. A. Bruining, G. J. Puppels, N. A. N. Thi, C. Kirschner, D. Naumann, D. Ami, A. M. Villa, F. Orsini, S. M. Doglia, H. Lamfarraj, G. D. Sockalingum, M. Manfait, P. Allouch and H. P. Endtz, *Appl. Environ. Microbiol.*, 2001, **67**, 1461.
- 34 D. Hutsebaut, K. Maquelin, P. De Vos, P. Vandenabeele, L. Moens and G. J. Puppels, *Anal. Chem.*, 2004, **76**, 6274.
- 35 M. Krause, B. Radt, P. Rösch and J. Popp, *J. Raman Spectrosc.*, 2007, **38**, 369.
- 36 M. Krause, P. Rösch, B. Radt and J. Popp, *Anal. Chem.*, 2008, **80**, 8568.
- 37 M. Harz, P. Roesch and J. Popp, *Cytometry, Part A*, 2009, **75A**, 104.
- 38 C. Xie, M. A. Dinno and Y.-S. Li, *Opt. Lett.*, 2002, **27**, 249.
- 39 Y.-S. Huang, T. Karashima, M. Yamamoto and H. Hamaguchi, *J. Raman Spectrosc.*, 2003, **34**, 1.
- 40 P. Rösch, M. Harz, M. Schmitt and J. Popp, *J. Raman Spectrosc.*, 2005, **36**, 377.
- 41 P. Rösch, M. Harz, K.-D. Peschke, O. Ronneberger, H. Burkhardt and J. Popp, *Biopolymers*, 2006, **82**, 312.
- 42 P. Rösch, M. Harz, K.-D. Peschke, O. Ronneberger, H. Burkhardt, A. Schuele, G. Schmauz, M. Lankers, S. Hofer, H. Thiele, H.-W. Motzkus and J. Popp, *Anal. Chem.*, 2006, **78**, 2163.
- 43 P. Rösch, M. Schmitt, W. Kiefer and J. Popp, *J. Mol. Struct.*, 2003, **661–662**, 363.
- 44 P. Rösch, M. Harz, M. Schmitt, K.-D. Peschke, O. Ronneberger, H. Burkhardt, H.-W. Motzkus, M. Lankers, S. Hofer, H. Thiele and J. Popp, *Appl. Environ. Microbiol.*, 2005, **71**, 1626.
- 45 M. Harz, P. Rösch, K.-D. Peschke, O. Ronneberger, H. Burkhardt and J. Popp, *Analyst*, 2005, **130**, 1543.
- 46 D. Naumann, S. Keller, D. Helm, C. Schultz and B. Schrader, *J. Mol. Struct.*, 1995, **347**, 399.
- 47 K. Maquelin, L.-P. i. Choo-Smith, T. Van Vreeswijk, H. P. Endtz, B. Smith, R. Bennett, H. A. Bruining and G. J. Puppels, *Anal. Chem.*, 2000, **72**, 12.
- 48 K. C. Schuster, I. Reese, E. Urlaub, J. R. Gapes and B. Lendl, *Anal. Chem.*, 2000, **72**, 5529.
- 49 K. C. Schuster, E. Urlaub and J. R. Gapes, *J. Microbiol. Methods*, 2000, **42**, 29.
- 50 A. P. Esposito, C. E. Talley, T. Huser, C. W. Hollars, C. M. Schaldach and S. M. Lane, *Appl. Spectrosc.*, 2003, **57**, 868.
- 51 C. Xie, Y.-Q. Li, W. Tang and R. J. Newton, *J. Appl. Phys.*, 2003, **94**, 6138.
- 52 W. E. Huang, R. I. Griffiths, I. P. Thompson, M. J. Bailey and A. S. Whiteley, *Anal. Chem.*, 2004, **76**, 4452.
- 53 G. Kawai, M. Ohnishi, Y. Fujino and Y. Ikeda, *J. Biol. Chem.*, 1986, **261**, 779.
- 54 G. Kawai, Y. Ikeda and K. Tubaki, *Agric. Biol. Chem.*, 1985, **49**, 2137.
- 55 H. Yamashita, S. Tsubokawa and A. Endo, *J. Antibiot.*, 1985, **38**, 605.
- 56 V. Mohacek-Grosev, R. Bozac and G. J. Puppels, *Spectrochim. Acta, Part A*, 2001, **57A**, 2815.
- 57 H. G. M. Edwards, N. C. Russell, R. Weinstein and D. D. Wynn-Williams, *J. Raman Spectrosc.*, 1995, **26**, 911.
- 58 K. De Gussem, P. Vandenabeele, A. Verbeke and L. Moens, *Spectrochim. Acta, Part A*, 2005, **61A**, 2896.
- 59 S. Stöckel, S. Meisel, R. Böhme, M. Elschner, P. Rösch and J. Popp, *J. Raman Spectrosc.*, 2009, **40**, 1469.
- 60 K. De Gussem, P. Vandenabeele, A. Verbeke and L. Moens, *Anal. Bioanal. Chem.*, 2007, **387**, 2823.
- 61 A. Naumann, M. Navarro-Gonzalez, S. Peddireddi, U. Kues and A. Polle, *Fungal Genet. Biol.*, 2005, **42**, 829.
- 62 A. Naumann, *Analyst*, 2009, **134**, 1215.
- 63 M. Baranska, H. Schulz, P. Roesch, M. A. Strehle and J. Popp, *Analyst*, 2004, **129**, 926.
- 64 A. Szeghalmi, S. Kaminskyj, P. Rösch, J. Popp and K. M. Gough, *J. Phys. Chem. B*, 2007, **111**, 12916.
- 65 R. Schweitzer-Stenner, *J. Raman Spectrosc.*, 2005, **36**, 276.
- 66 K. Hering, D. Cialla, K. Ackermann, T. Doerfer, R. Moeller, H. Schneidewind, R. Mattheis, W. Fritzsche, P. Roesch and J. Popp, *Anal. Bioanal. Chem.*, 2008, **390**, 113.
- 67 A. Zumbusch, G. R. Holtom and X. S. Xie, *Phys. Rev. Lett.*, 1999, **82**, 4142.
- 68 J.-X. Cheng, Y. K. Jia, G. Zheng and X. S. Xie, *Biophys. J.*, 2002, **83**, 502.
- 69 T. Meyer, D. Akimov, N. Tarcea, S. Chatzipapadopoulos, G. Muschiolik, J. Kobow, M. Schmitt and J. Popp, *J. Phys. Chem. B*, 2008, **112**, 1420.
- 70 G. Bergner, S. Chatzipapadopoulos, D. Akimov, B. Dietzek, D. Malsch, T. Henkel, S. Schlücker and J. Popp, *Small*, 2009, **5**, 2816.
- 71 D. Akimov, S. Chatzipapadopoulos, T. Meyer, N. Tarcea, B. Dietzek, M. Schmitt and J. Popp, *J. Raman Spectrosc.*, 2009, **40**, 941.
- 72 M. Müller and A. Zumbusch, *ChemPhysChem*, 2007, **8**, 2156.
- 73 B. von Vacano, W. Wohlleben and M. Motzkus, *J. Raman Spectrosc.*, 2006, **37**, 404.
- 74 C. Krafft, B. Dietzek and J. Popp, *Analyst*, 2009, **134**, 1046.
- 75 C. Krafft, A. Ramoji Anuradha, C. Bielecki, N. Vogler, T. Meyer, D. Akimov, P. Rösch, M. Schmitt, B. Dietzek, I. Petersen, A. Stallmach and J. Popp, *J. Biophotonics*, 2009, **2**, 303.
- 76 D. J. Niederpruem and D. P. Hackett, *Plant Physiol.*, 1961, **36**, 79.
- 77 D. Schubert, M. Raudaskoski, N. Knabe and E. Kothe, *Eukaryotic Cell*, 2006, **5**, 683.
- 78 K. Kolo and P. Claeys, *Biogeosciences*, 2005, **2**, 277.
- 79 D. Merten, E. Kothe and G. Buechel, *Mine Water Environ.*, 2004, **23**, 34.
- 80 P. Lasch, W. Haensch, D. Naumann and M. Diem, *Biochim. Biophys. Acta*, 2004, **1688**, 176.
- 81 R Development Core Team, *R: A Language and Environment for Statistical Computing*, R Foundation for Statistical Computing, Vienna, Austria, 2008.
- 82 B. Westermann and H. Prokisch, *Fungal Genet. Biol.*, 2002, **36**, 91.
- 83 N. N. Levina and R. R. Lew, *Fungal Genet. Biol.*, 2006, **43**, 65.

- 84 F. Fuchs, H. Prokisch, W. Neupert and B. Westermann, *J. Cell Sci.*, 2002, **115**, 1931.
- 85 D. P. McDaniel and R. W. Roberson, *Fungal Genet. Biol.*, 2000, **31**, 233.
- 86 A. C. Williams and H. G. M. Edwards, *J. Raman Spectrosc.*, 1994, **25**, 673.
- 87 J. De Gelder, K. De Gussem, P. Vandenabeele and L. Moens, *J. Raman Spectrosc.*, 2007, **38**, 1133.
- 88 A. T. Tu, *Raman Spectroscopy in Biology: Principles and Applications*, John Wiley & Sons, New York, 1982.
- 89 T. Kitagawa, Y. Kyogoku, T. Iizuka, M. Ikeda-Saito and T. Yamanaka, *J. Biochem.*, 1975, **78**, 719.
- 90 V. Escriou, F. Laporte, P. V. Vignais and A. Desbois, *Eur. J. Biochem.*, 1997, **245**, 505.
- 91 J. K. Hurst, T. M. Loehr, J. T. Curnutte and H. Rosen, *J. Biol. Chem.*, 1991, **266**, 1627.
- 92 S. Hu, I. K. Morris, J. P. Singh, K. M. Smith and T. G. Spiro, *J. Am. Chem. Soc.*, 1993, **115**, 12446.
- 93 F. Adar and M. Erecinska, *Biochemistry*, 1978, **17**, 5484.
- 94 C. Matthäus, T. Chernenko, J. A. Newmark, C. M. Warner and M. Diem, *Biophys. J.*, 2007, **93**, 668.
- 95 V. V. Pully and C. Otto, *J. Raman Spectrosc.*, 2009, **40**, 473.